A Novel Low-loss Integrated 60 GHz Cavity Filter with Source-Load Coupling using Surface Micromachining Technology

Bo Pan, Yuan Li, Manos M. Tentzeris, and John Papapolymerou

Abstract—This paper presents a novel surface micromachined low-loss integrated cavity filter with a pair of transmission zeros using a simple source-load coupling scheme for emerging 60 GHz applications. The proposed method eliminates the dielectric loss by elevating the cavity-based filter into the air with the aid of the polymer-core conductor surface micromachining technology. The electrical fields of the cavity are thus entirely in air. A coplanar waveguide input and output interface is designed for easy integration with other planar electronics. The inter-cavity inductive coupling is realized through the use of pillar array iris, with the source-load capacitive coupling achieved with integrated coplanar waveguide lines. This combination of couplings creates a pair of transmission zeros to help achieve better selectivity. A measured insertion losses as low as 1.92 dB, along with a pair of transmission zeros, has been observed at 60 GHz.

Index Terms—millimeter wave, *V*-band, surface micromachining, integrated cavity filter, transmission zeros, source-loading coupling

I. INTRODUCTION

Integrated waveguide filters have demonstrated great potential for millimeter wave applications, in terms of insertion loss, fabrication accuracy, power handling capability and frequency selectivity [1]- [5]. Silicon bulk micromachining technologies and multi-layer LTCC/LCP/PCB technologies have been used in these filters. To enhance the stopband rejection performance, transmission zero synthesis techniques, have been also introduced in the design of the integrated waveguide filters [6]- [9]. These include introducing cross coupling between non-adjacent cavities, dual mode operations, non-resonating nodes and source-load coupling. Among them, the source-load coupling scheme can create two transmission zeros by using only two cavities that lead to a more compact design. Its synthesis methods, along with different implementation schemes, have been reported in [10]- [13].

In this paper, an integrated cavity filter is implemented by using SU-8 based polymer-core conductor surface micromachining technology [14], [15]. By elevating the cavity-based filter and its electrical fields entirely into the air, the proposed method eliminates the dielectric loss. Rows of metallized polymer pillars that are patterned by a standard photolithography on the top of the substrate form the cavity sidewalls. The bottom of the cavity is formed by metalizing the substrate's top surface, while the top is formed by a separate micromachined piece. Unlike other existing solutions that require either a bulk-micro-machine-able or a low loss via-hole technology compatible substrate, the proposed method is
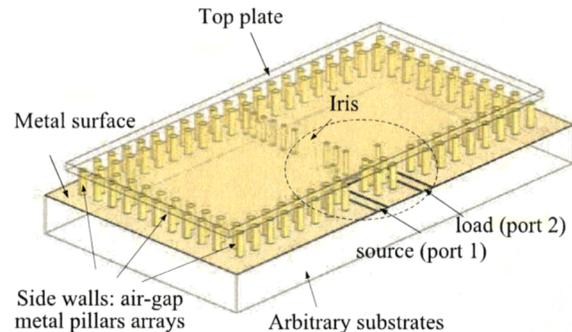

Fig. 1. Concept drawing of the proposed filter structure (detailed structures in the dashed circle is shown in Fig. 2).
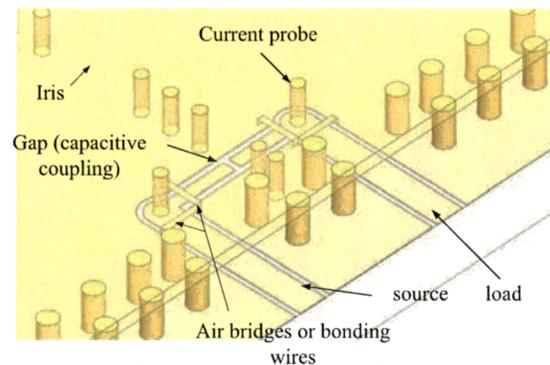

Fig. 2. Feeding and coupling schemes for the proposed filter.

a substrate independent integration approach and can be built on top of lossy substrates such a doped silicon wafer used in IC fabrication. Moreover, it provides a compact coplanar waveguide input/output interface and, thus, is fully compatible with monolithic integration of other planar components in a System-On-a-Chip approach.

A simple source-load coupling scheme is introduced by using a coplanar waveguide gap between the source and the load. The inter-cavity inductive coupling is realized by a pillar array iris. This combination of couplings creates a pair of transmission zeros to help achieve better selectivity.

A 60 GHz second-order prototype filter was built to demonstrate multiple advantages brought by the proposed method since 60 GHz has drawn a lot of attention for WPAN and
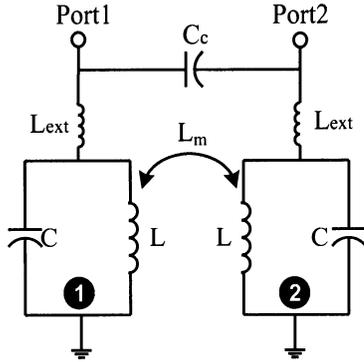
Fig. 3. Equivalent circuit model for the proposed source-loading coupling 2-pole filter

Fig. 4. S_{21} as the function of the CPW gap in source load capaciti e coupling

wireless multimedia applications. A measured insertion loss as low as 1.92 dB, along with a pair of transmission zeros located at 58.3 and 60.8 GHz were observed. This design can be easily scaled to even higher frequency bands for emerging sub-millimeter wave applications, while maintaining its superior performances.

II. DESIGN AND FABRICATION

Fig. 1 shows the proposed filter structure. Fig. 2 shows the source-loading coupling detail. Unlike a substrate integrated waveguide (SIW) where rows of vias are located inside the substrate, here, metalized rows of pillars are located on top of the substrate, with air gaps between them, to form a band-gap structure at the frequency of interest [16]. In this paper, two rows of pillars form the side walls of the elevated cavity/waveguide and are sufficient to block the leakage from the air gaps between the pillars. The top plate is a separate met-alized piece stacked on top of pillars and the bottom plate is the metallization on the top of substrate. The underneath substrate only plays the role of mechanically supporting medium. In Fig. 1 , the top plate is shown as a transparent frame to reveal the details inside.

In the proposed technology, cores of pillar arrays are formed through patterning a thick photo-definable polymer SU-8, and then plating their outer surface up to several microns. Compared with traditional via-hole plating used in an SIW, the proposed method is more economical. Although it is possible to directly pattern solid walls, pillar fences are used instead due to the fabrication feasibility concern, which has been discussed in [15].

The equivalent circuit model of the proposed two-pole transmission zero filter is shown in Fig. 3. The circuit con-sists of two shunt LC resonators representing two cavities, a mutual coupling inductor L_m representing the inductive coupling between two cavities, a capacitor C_c connecting the source and the load to provide an electrical coupling that has an opposite sign compared with the inductive coupling, and two inductors L_{ext} that represent the external coupling current probes. A pair of transmission zeros out of the
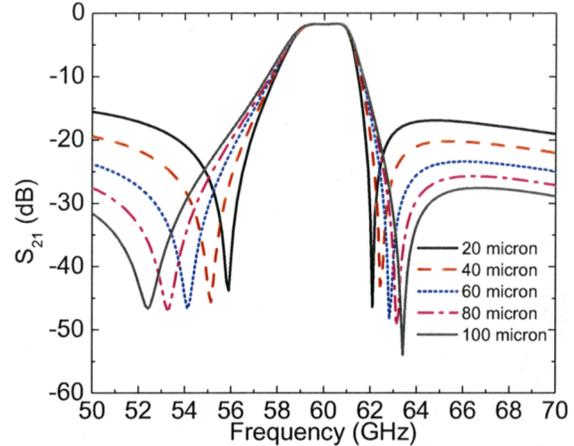
passband can be created when there is a 180° phase differ-ence between two paths($Path1$: source → capacitor→load; $Path2$: source→current probe→cavity 1→iris coupling→cavity 2→current probe→load). Details of the phase delay calculations can be found in [11].

The inductive coupling between the two cavities is imple-mented by the pillar iris and the capacitive coupling is realized in a planar form instead, using a gap formed by two CPW stubs as shown in Fig. 2. To form the CPW gap between the source and the load, the spacing between two pillars has to be increased to allow sufficient space for CPW routing. The impact on the inductive coupling between the cavities, from this increased pillar spacing, has been taken into account in the full-wave simulations. The locations of the transmission zeros can be controlled by varying the gap; it essentially changes the coupling capacitance between the source and the load. The simulated filter responses as a function of the gap are plotted in Fig. 4. As can be seen, the smaller the gap, the closer the transmission zeros from the passband. A smaller gap means a larger coupling capacitance, leading to a closer-to-passband transmission cancellation from the two different paths.

The external coupling is achieved through a current probe connected to a CPW line. The probe contacts the top wall of the cavity and excites it using magnetic coupling. The external coupling level is controlled by the probe position. The relationship between the external quality factor Q_{ext} and the physical positions of the feeding probe can be found in [17]. The inter-cavity coupling level is controlled by the iris opening and its design curve can be found in any waveguide filter design handbook.

A prototype filter is designed for proof of concept in this research. The design center frequency is set as 60 GHz and the 3-dB fractional bandwidth is chosen as 1 GHz. A solid wall version is designed first to reduce the full-wave simulation time and then transformed into pillar arrays using the following equation:
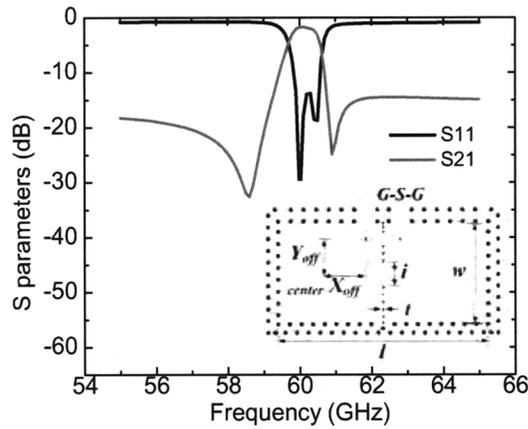
Fig. 5. Optimized filter response and illustration of physical dimensions

TABLE I
OPTIMIZED FILTER DIMENSIONS.

(Units: mm)

Dimensions	Value	Dimensions	Value
l	7.3	i	0.8
w	3.5	t	0.1
X_{off}	1.05	gap	0.05
Y_{off}	1.6	pitch	0.44
diameter	0.14		

$$W_{eff} = W - d^2/0.95b \qquad (1)$$

where W_{eff} is the width of the equivalent solid-wall cavity that has the same resonant frequency. W is the measured center-to-center distance between the two inner rows of pillars (as shown on the inset in Fig. 5). d is the diameter of the pillar and b is the pitch between two adjacent pillars. d and b were chosen to minimize the EM-wave leakage while meeting the fabrication constraints [16]. The inductive iris is formed by only one row of pillars since it will not introduce leakage to the outside of the cavity. Different diameters are chosen for sidewall pillars and inter-cavity pillars to effectively block EM-wave leakage and reduce the chip real estate.

To facilitate on-wafer probe measurement, CPW lines from the source and the load (as shown in Fig. 2) are bent and carefully routed to minimize parasitic effects.

Fig. 5 shows the full wave simulated performances by Ansoft HFSS for the proposed filter with the dimensions shown in Table 1. A 1.7 dB pass-band insertion loss is found in the simulations, taking into account the metal loss (with finite metal roughness) and radiation leakage. Two transmission zeros are located at 58.6 GHz and 60.9 GHz respectively.

Fig. 6 details the fabrication process steps [14] [15]: a thin Ti layer was sputtered to improve the SU-8's adhesion to the glass. A negative photo-definable epoxy SU-8 2035 300 μm thick was dispensed and patterned to define the cores of the pillar fences. Ti/Cu/Ti was then sputtered as the seed layer to cover the pillars, as well as the substrate
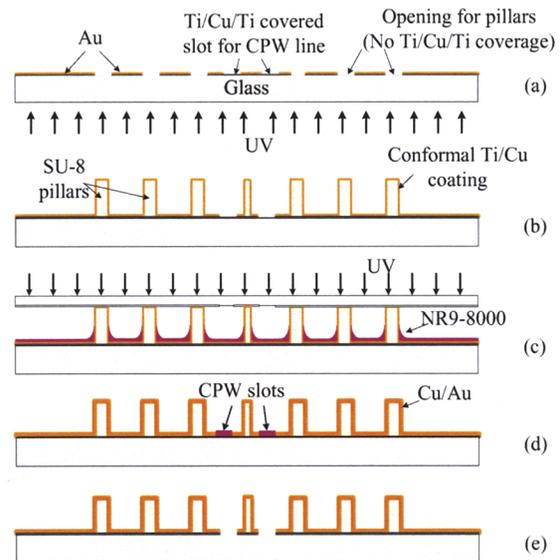

Fig. 6. Fabrication flow of the proposed air-lifted cavity resonator filter.

in a conformal manner. Negative photo-resist NR9-8000 was coated and patterned in a non-contact way to cover the CPW slot region, preventing the metal coverage on the slot in the following electroplating step. Electroplating of copper and gold covers the sidewall of the pillars and the exposed feeding structures. A piece of silicon wafer was metallized to be used as a top plate of the cavity and bonded with the pillars using silver paste. An SEM picture of a fabricated sample shows the capacitive coupling gap between the source and the load in Fig.7 (a) . Pillars with a smaller diameter are used for inductive iris and feeding probes, while larger ones for the sidewall. Al/Si wedge bonding wires are used to connect the CPW grounds preventing parasitic slot-mode radiation. An SEM picture of a bonding wire is shown in Fig.7 (b).

III. MEASUREMENT

The fabricated sample on a glass substrate is measured by an Agilent 8510XF vector network analyzer station connected with GSG probes of a 250 μm pitch. The reference plane was set to the outer surface of the sidewall. The measurement results are plotted in Fig. 8.

Good agreement between the simulation and the measurement is observed, as shown in Table II. A slight frequency shift (less than 0.17 %) to a lower band (from 60.14 GHz to 60.04 GHz) was observed and might be explained by numerical errors in the simulations. Two transmission zeros are observed at 58.3 and 60.8 GHz. A 1.92 dB insertion loss and a return loss greater than 15 dB were achieved for the fabricated prototype.

IV. CONCLUSIONS

In this paper, a novel approach to implement source-load coupling high performance integrated waveguide filters using polymer-core conductor surface micromachining technology is
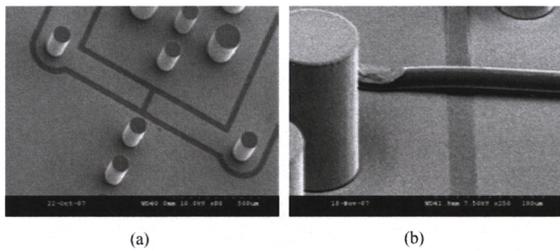
Fig. 7. SEM pictures of (a) feeding and source-load coupling before wire-bonding.(b) a bonding wire span over a CPW slot.
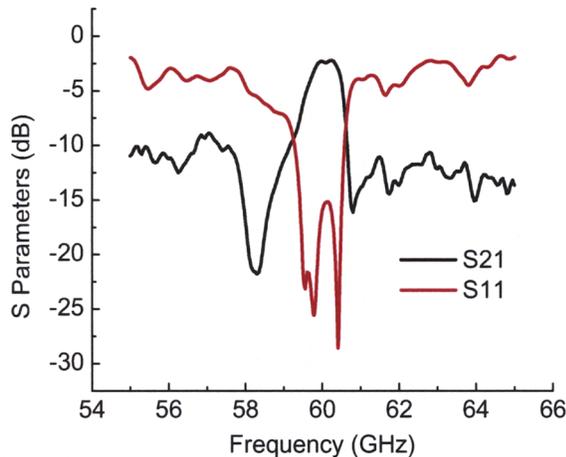

Fig. 8. Measurement results of the fabricated source-load coupling filter

presented. By elevating a cavity filter on top of the substrate and using air as the filler, the dielectric loss can be eliminated. An insertion loss as low as 1.92 dB for a two-pole transmission zero filter with a simple capacitive coupling scheme has been observed for a benchmarking prototype on glass at around 60 GHz. The proposed method also offers an easy integration of both planar components and 3-D integrated modules on top of the substrate.

REFERENCES

[1] L. Katehi, G. Rebeiz, T. Weller, R. Drayton, H. Cheng, J.Whitaker, "Micromachined circuits for millimeter- and sub-millimeter-wave applications", *IEEE Antennas and Propagation Magazine*, Vol. 35, No. 5, pp 9-17, Oct. 1993.

[2] W. McGrath, C. Walker, M. Yap, Y.-C. Tai, "Silicon micromachined waveguides for millimeter-wave and submillimeter-wave frequencies", *IEEE Microwave and Wireless Components Letters*, Vol. 3, No. 3, pp. 61-63, March 1993.

[3] Y. Lee, J. P.Becker, J. R. East, and L. P. B. Katehi, "Fully micromachined finite-ground coplanar line-to-waveguide transitions for W-band applications," *IEEE Trans. Microw. Theory Tech.*, vol. 52, no. 3, pp. 1001-1007, Mar. 2004.

[4] D. Deslandes and K. Wu, "Integrated microstrip and rectangular waveguide in planar form," *IEEE Microw. Wireless Compon. Lett.*, vol. 11, no. 2, pp. 68-70, Feb. 2001.

[5] D.Stephens, P. Young, I. Robertson, "Millimeter-wave substrate integrated waveguides and filters in photoimageable thick-film technology", *IEEE Transactions on Microwave Theory and Techniques*, Vol. 53, No. 12, pp. 3832-3838, Dec. 2005.

[6] J.-S. Hong and M. J. Lancaster, *Microstrip Filters for RF/Microwave Applications*. New York: Wiley, 2001.

[7] R. Cameron, "Advanced coupling matrix synthesis techniques for microwave filters", *IEEE Transactions on Microwave Theory and Techniques*, Vol. 51, No. 1, Part 1, pp. 1-10, Jan. 2003.

[8] E. Ofli, R. Vahldieck, S. Amari, "Novel E-plane filters and diplexers with elliptic response for millimeter-wave applications", *IEEE Trans. on Microwave Theory and Techniques*, Vol. 53, no. 3, Part 1, pp. 843-851, March 2005.

[9] J. Ruiz-Cruz, M. Sabbagh, K.A. Zaki, J.M. Rebollar, Y. Zhang, "Canonical ridge waveguide filters in LTCC or metallic resonators", *IEEE Transactions on Microwave Theory and Techniques*, Vol. 53, No. 1, pp 174 -182, Jan. 2005.

[10] S. Amari,"Direct synthesis of folded symmetric resonator filters with source-load coupling"; *IEEE Microwave and Wireless Components Letters*, Vol. 11, No. 6, pp 264-266, June 2001.

[11] J.-H.Lee, S.Pinel, J.Laskar, and M.M.Tentzeris, "Design and Development of Advanced Cavity-Based Dual-Mode Filters Using Low-Temperature Co-Fired Ceramic Technology for V-band Gigabit Wireless Systems", *IEEE Transactions on Microwave Theory and Techniques*, Vol.55, No.9, pp.1869-1879, September 2007.

[12] Sanghoon Shin, R. Snyder, "At least N+1 finite transmission zeros using frequency-variant negative source-load coupling", *IEEE Microwave and Wireless Components Letters*,Vol. 13, No. 3,pp 117 - 119, March 2003.

[13] L.K. Yeung and Ke-Li Wu, "A compact second-order LTCC Bandpass Filter with Two Finite Transmission Zeros", *IEEE Trans. on Microwave Theory and Techniques*, Vol. 51, no. 2, pp. 337-341, Feb. 2005.

[14] Y-K. Yoon, J-W. Park and M. G. Allen, "Polymer-core conductor approaches for RF MEMS," *Journal of Microelectromechanical Systems*, vol. 14, No. 5, pp. 886-894, Oct. 2005.

[15] B. Pan, Y. Li, M. M Tentzeris and J. Papapolymerou, "A High-Q Millimeter-Wave Air-lifted Cavity Resonator on Lossy Substrates", *IEEE Microwave and Wireless Components Letters*, Vol. 17, No. 8, pp 571 - 573, Aug. 2007.

[16] D. Deslandes and K. Wu, "Accurate Modeling, Wave Mechanisms, and Design Considerations of Substrate Integrated Waveguide", *IEEE Trans. Microwave Theory Tech.*, vol. 54, pp. 2516-2526, June 2006.

[17] B. Pan, Y. Li, M. M Tentzeris and J. Papapolymerou, "High Performance Surface Micromachined Millimeter-Wave Cavity Filters", submitted to *IEEE Transaction on Microwave Theory and Tech.*

TABLE II
COMPARISON OF SIMULATED AND MEASURED RESPONSES

(Units: GHz)

	center	3-dB BW	pole 1	pole 2	zero 1	zero 2
sim	60.14	1.0	60	60.5	58.6	60.9
meas	60.04	1.1	59.8	60.4	58.3	60.8